2018 European Control Conference (ECC)
June 12-15, 2018. Limassol, Cyprus

A Low-Cost System for Dynamic Analysis of Pupillary Light Response for a Driver Drowsiness Detection System

Alessandro Amodio, Michele Ermidoro, Davide Maggi, Sergio Matteo Savaresi, *Senior Member, IEEE,*

***Abstract*— This paper proposes a low-cost methodology for analyzing the dynamics of constriction of a human pupil while subjected to a light stimulus: this phoenomenon is commonly known as Pupillary Light Reflex (PLR) and is widely utilized in medical field to diagnose a variety of diseases. In particular, the analysis of the PLR in this paper is preparatory to the development of a Driver Drowsiness Detection System (DDDS), which reveals the driver's sleepiness state by measuring the pupil's constriction dynamics. The test protocol consists in applying a light stimulus to one eye of the subject and to capture the dynamics of constriction of both eyes through cameras; the proposed methodology extracts from the video sequences the time profile of the pupil diameter, from which dynamic and static features are obtained by fitting a simplified 1^{st}-order model with delay. Finally, conclusions on the intra- and inter-subject variability of such features are drawn and possible DDDS strategies are proposed based on the obtained results.**

I. Introduction and Motivation

According to the World Health Organization [1], nowadays road accidents are among the top-10 causes of death, and the only one which is not a disease; moreover, several in-depth studies [2], [3] revealed the impact of drowsiness on road accidents to be around $10\% - 20\%$ of the total.

The so-called Advanced Driver Assistance Systems (ADAS, [4]), are in-vehicle systems designed to operate in common driving scenarios and to intervene or simply provide an alert to the driver every time a dangerous situation is about to occur. ADAS are becoming more and more popular in the scientific community and can be classified into two categories: active, when capable of influencing the vehicle dynamics, and passive, when only able of providing information/alert to the driver. Examples of the former type is the Adaptive Cruise Control [5] and the Road Departure Avoidance [6]; examples of the latter are the and the Lane Change Decision Aid Systems (LCDAS, [7]) and the Driver Drowsiness Detection Systems (DDDS).

Among the ADAS, the DDDSs are in charge of monitoring driver and/or vehicle behavior, evaluate some performance indices, and provide alerts or stimulation if the driver seems to be too drowsy [8]. A number of solutions with different methods have been proposed so far, which can be subdivided, depending on the technology, into the following three categories:

1) methods based on biomedical signals, like cerebral, muscular and cardiovascular activity;
2) methods based on driver behavior, which evaluate the driving pattern, the velocity, the steering wheel angle and other signals;
3) methods based on driver visual analysis using image processing techniques.

The main solutions belonging to the first category [9], [10], [11], [12] currently require sensors to be attached to the driver's body, which makes them hard to implement on industrial scale.

The signals required by the second approach are much easier to acquire, leading it to be the most widespread in the commercial market. The main limitations are related to the sensitivity to vehicle type, driver experience, geometric characteristics, condition of the road and so on; moreover, analyzing the user behavior commonly requires a great computational effort, and provides poor performance in case of the so-called micro-sleeps, that is when a drowsy driver falls asleep for a few seconds on a very straight road section without changing the vehicle signals [13].

The third approach relies on the acquisition of driver's images through video-cameras placed in front of the user, which makes the computer vision-based techniques less intrusive than the first approach. The idea at the basis of the this method is to exploit the clear connection between the occurrence of sleepiness and the driver's face appearance and head/eyes activity. The computer vision-based techniques have attracted great interest in the scientific community so far, with a number of proposed solutions based on indices such as percentage of eye closure [14] or head movement [15]. However, not many commertial products exploiting this technology can be currently found on the market; to the authors knowledge, the only implementation on a commercial vehicle of a DDDS that exploits driver visual analysis is represented by the DS Driver Attention Monitoring System on the DS7 Crossback.

The involuntary reflex of the human pupil reacting to an increase of light condition is called Pupillary Light Reflex (PLR) and is widely utilized in the medical field as a diagnostic tool for a variety of possible lesions and impairment conditions. This paper proposes a preliminary study to the development of a DDDS based on a computer vision-based approach: the goal is to detect the drowsiness of a driver based on a dynamic analysis of the subject's PLR through video acquisitions and image processing techniques. In particular, a stepwise light stimulus is applied to one eye of a subject and the PLRs are evaluated by video-recording the pupil constriction dynamics of the Illuminated Eye (IE) and of the Not Illuminated Eye (NIE). The driver's drowsiness can thus be evaluated by comparing such information to baseline values.

The main contribution of this paper is the design and

978-3-9524-2699-9 ©2018 EUCA

implementation of a low-cost system for performing PLR dynamic analysis for a DDDS. At first, a simple model for such dynamics is proposed; then, a methodology is presented for extracting the time profile of the pupil diameter from video sequences. A set of dynamic and static features is in turn extracted from such time profiles and a final evaluation of the obtained results is performed in terms of intra- and inter-subject variability; a simple DDDS strategy is finally proposed based on the obtained results.

The paper is organized as follows: Section II discusses the different causes of pupil size variations and proposes a mathematical model of the system. Section III contains a description of the experimental set-up and of the test protocol and Section IV describes the methodology for extracting the features of interest from the video sequences. Finally, Section V presents the esperimental results and Section VI the conclusions.

II. Pupil Dynamics and Modeling

This Section includes a short description of the pupil and of the main causes of pupil size variation; finally, a simple mathematical model is introduced to describe the dynamics of interest.

The pupil is a hole located in the center of the iris. The light enters the eye passing through the pupil and then strikes the retina; it appears black mainly because the entering light rays are absorbed by the tissues inside the eye. The pupil is the eye's part that is responsible for the regulation of the light reaching the retina: it constricts when the light amount increases and, viceversa, dilates in case of low-light condition to always ensure optimal light amount striking the retina.

Many reasons may cause pupil diameter variations. First, the pupil size undergoes spontaneous oscillations, which is a normal and persistent behavior in every subject, occurring without any stimulation. Pupil size variations may also be due to involuntary reflex reactions, such as the Accomodation Reflex or the Light Reflex. The Accomodation is a constriction or dilation of the pupil in response to focusing on a near object or looking to a distant one respectively; in these cases, the pupil responds in order to always guarantee best focus condition. The Light Reflex can be Direct or Consensual; the Direct Light Reflex is occurs when the eye is subject to a light stimulus and causes pupil constriction. If the subject is healthy, the sizes of the two pupils are always kept approximately at the same value by the Consensual Light Reflex, responsible of the constriction of a pupil, when the other one constricts due to Direct Light Reflex. A pupil size variation can also be induced by other factors, such as emotional stimuli, i.e. by recalling a particularly emotional event [16] or by subliminal auditory stimuli [17].

In this paper, a light stimulus is applied to one eye of a subject, inducing a Direct Light Response to that eye and the Consensual Light Response to the other. Several models can be found in literature for describing the dynamics of the PLR [18], [19]; the Kohn and Clynes model is widely utilized and considers both the "fast" and "slow" dynamics, in dependence on whether a positive or negative light stimulus is applied. In this study, only the fast dynamics due to positive light stimuli is taken into account; this allows to consider a simple model, linearized in the vicinity of the equilibrium condition representing the instant immediately before the light stimulus application. The considered parametric grey-box model can be represented by the following 1^{st}-order transfer function with time delay, modeling the dynamics from the light amount reaching the retina to the pupil diameter:

$$G(s) = \frac{\mu e^{-\tau s}}{1+Ts}. \tag{1}$$

The model contains the following parameters, which are constrained due to the physics of the system as described in the following:

- gain: $\mu \leq 0$;
- delay: $\tau \geq 0$;
- time constant: $T > 0$.

The gain must be non-positive because, to a positive light step (which, by convention, describes a light amount increase) always corresponds a pupil size decrease. The time constant must be positive since the system is known to be stable and delay must be non-negative in order to maintain a physical meaning.

Each model belonging to this class can be associated to the row vector of parameters $\phi = [\mu, \tau, T]$; the set of all such models satisfying the abovementioned constraints is indicated by Φ and is described in the following:

$$\Phi = \{[\mu, \tau, T] \in \mathbb{R}^3 \,|\, \mu \leq 0, \tau \geq 0, T > 0\}. \tag{2}$$

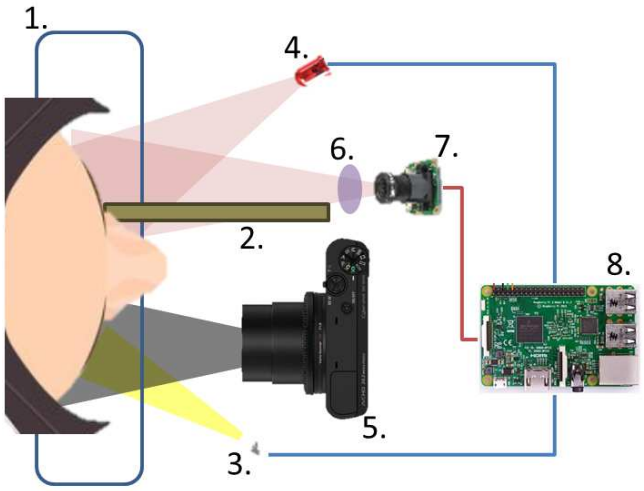

Fig. 1: Experimental Set-up

III. Experimental Set-Up and Test Protocol

Fig. 1 graphically describes all the components of the experimental set-up, which are summarized in the following together with the test protocol.

1) face support;
2) separator;

3) visible light LED;
4) infrared light LED;
5) visible-spectrum camera;
6) infrared filter;
7) full-spectrum camera;
8) board for video acquisition and LEDs control.

For each test, the subjects are asked to position their face on the support (item 1.), which ensures optimal and constant positioning, for improving test repeatability. Then, in a completely dark ambient, a train of three light impulses, 4 seconds long, at intervals of 10 seconds from each other is generated; each light impulse is achieved by a couple of LEDs, a visible-light one (item 3.) directed to one eye, and an infrared one (item 4.) directed to the other eye. A separator (item 2.) ensures that no visible light falls into the NIE, in order to minimize pupil constriction due to Direct Light Reflex for this eye. The pupil constriction relative to the visible light-illuminated eye is recorded with a standard $100\,fps$ camera, while the other is recorded with a full-spectrum $100\,fps$ camera (item 7.) equipped with an infrared filter (item 6.) to improve the image quality by enhancing the IR content. Finally, an electronic board (item 8.) drives the LEDs and controls the two cameras.

IV. Data Processing

In this Section, the method for extracting dynamic and static information on the subject's PLR from video sequences is presented. The methodology can be subdivided into three steps, which are described in the following.

(a) IE and NIE videos synchronization;
(b) video extraction of time profiles of the pupils size;
(c) model identification and features extraction.

A. IE and NIE Videos Synchronization

For each test a couple of video sequences is acquired with separate cameras, one for each eye; the first operation is thus the synchronization of the two videos.

The test is performed in dark condition and, for each light step, the control board drives the two LEDs (visible and infrared light) in the same instant; in this way, it's possible to set the zero-instant in both videos when the respective image is illuminated. The problem then moves to detecting the first illuminated frame of a video sequence; we denote with R, G and B the average values of the red, green and blue channels of an image pixels, and compute the luminance of an image as follows:

$$\begin{aligned} \lambda &= \alpha * R + \beta * G + \gamma * B \\ s.t. \quad & \alpha + \beta + \gamma = 1. \end{aligned} \tag{3}$$

By choosing different $[\alpha, \beta, \gamma]$ combinations satisfying the constraint in Eq. 3, many definitions of luminance can be obtained; a simple and popular one is for example $[\frac{1}{3}, \frac{1}{3}, \frac{1}{3}]$. In order to detect the instant in which the LEDs light up, a luminance threshold λ_T is selected and the zero-instant is determined for both videos as the first frame satisfying:

$$\alpha * R + \beta * G + \gamma * B \geq \lambda_T. \tag{4}$$

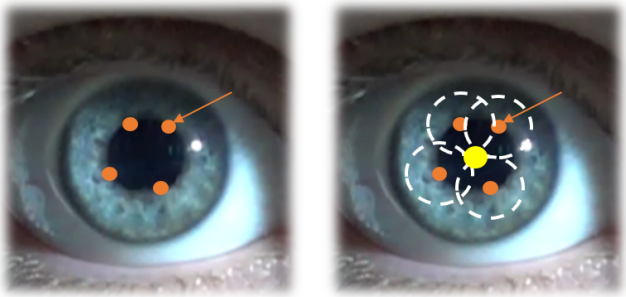

(a) (b)

Fig. 2: Circular Hough Transform

B. Pupil Size Extraction from Video

The problem of detecting iris [20] and pupil [21] within an image has been widely investigated in the scientific literature, and the Circular Hough Transform (CHT) is among the most utilized techniques. Given the desired radius, the method finds all circles within the image with that radius and returns their position: the main steps are summarized in the following.

1) Candidate pixels that are supposed to lie on the circle are selected as the high-gradient ones within the image and are thus allowed to "cast votes" (Fig. 2a, red dots) to select the center.
2) Each candidate votes every pixel that lies at a distance given by the pre-determined radius (Fig. 2b, white dashed circles).
3) The pixel where the most votes accumulate is the selected center (Fig. 2b, yellow dot).

In this paper, a CHT-based algorithm is employed to extract the pupil size profile from video sequences; the algorithm takes as input a range of circle radii and returns the position and radius of the circle that accumulates the most votes and whose radius falls within the desired range.

The algorithm is described by the following steps:

1) A first image crop is performed in order to isolate the eye of interest from the rest of the image; this operation is sufficiently robust thanks to the face support (item 1. in Fig. 1), that ensures correct positioning at each test, guaranteeing that the eye always lies in the same section of the image.
2) At each frame, the algorithm searches the iris and pupil within the cropped image; when the detections are stable for a fixed number of frames, the algorithm stores the iris size and moves to the following step.
3) A second image crop is performed in order to isolate the pupil, while the iris is discarded. The circle radius range is adapded to account for pupil constriction during the test and the crop area is also adaptively changed to follow potential movements of the eye.

C. Model Identification and Features Extraction

The blue dots in Fig. 3 show the result of the process described in Section IV-B, where the estimated pupil diame-

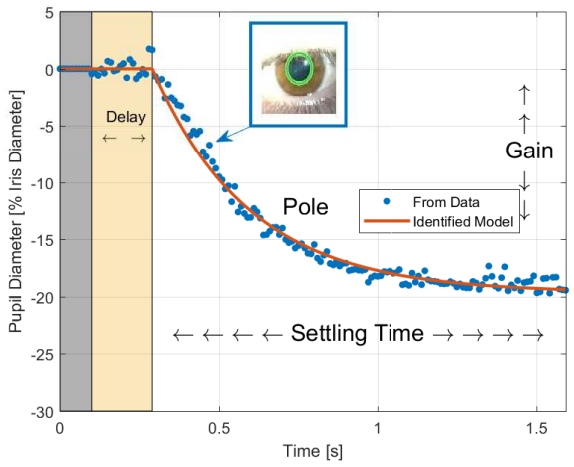

Fig. 3: Model Identification

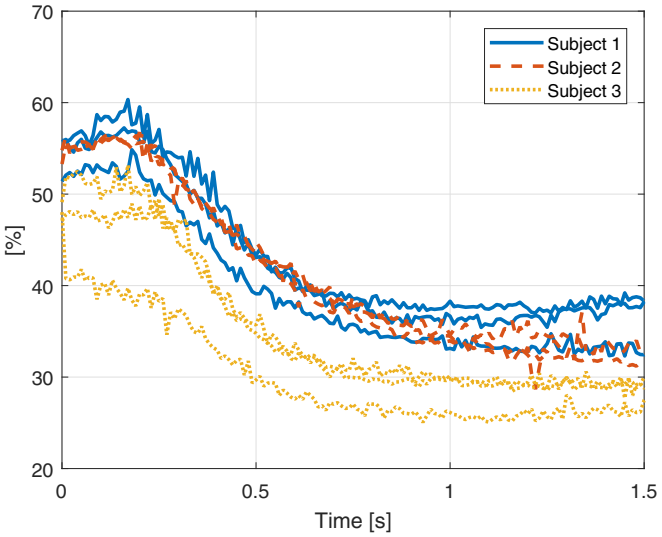

Fig. 4: Time domain analysis - IE

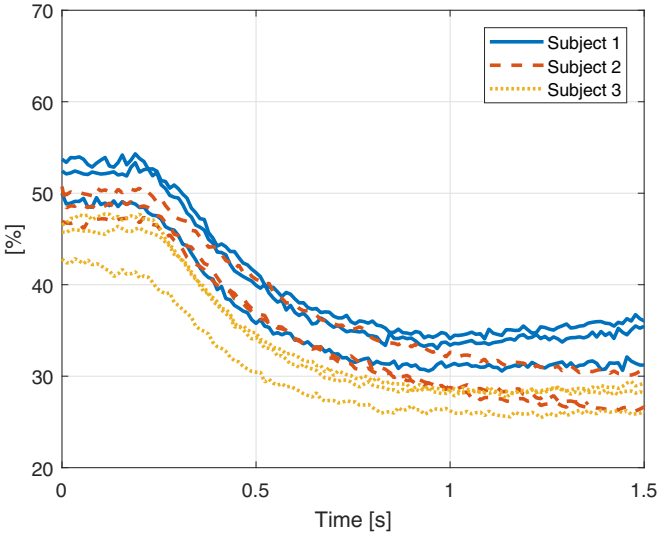

Fig. 5: Time domain analysis - NIE

ter is expressed in terms of percentage of the iris diameter; a light impulse is applied after $0.1\,s$ (the grey region represents the dark condition) and, after some delay (yellow region), the pupil responds with a diameter reduction.

After deriving the time profile of the pupil size from each of the video sequences, a model of the class described in Eq. 1 is obtained by parametric identification from the data. For each time profile of the pupillary response, the first $1.5\,s$ are extracted and then the parameters $\phi^* = [\mu^*, \tau^*, T^*]$ that ensure optimal fitting are computed by solving a least-squares curve fitting problem. Supposing N to be the total number of considered samples, if we denote by $y(k), k = 1,...,N$ the computed values of the pupil diameter in each sample and $\hat{y}(k,\phi)$ the step response of the model ϕ at instant k, ϕ^* is determined as follows:

$$\phi^* = \arg\min_{\phi \in \Phi} \sum_{k=1}^{N} [\hat{y}(k,\phi) - y(k)]^2. \tag{5}$$

Without loss of generality, the step amplitude for computing the model step response is taken as 1. The result of this optimization performed on a sample pupillary response test is shown in Fig. 3, where the red line is the estimated model's step response.

In order to evaluate the characteristics of the PLR, the eight-element feature vector $\varphi = [\mu_{IE}, \mu_{NIE}, \tau_{IE}, \tau_{NIE}, \omega_{IE}, \omega_{NIE}, t_{IE}, t_{NIE}]$ is associated to every step response. This vector contains the gains of the identified models for the IE and NIE (μ_{IE}, μ_{NIE}), together with the relative delays (τ_{IE}, τ_{NIE}) and pole frequencies ($\omega_{IE}, \omega_{NIE}$). Moreover, the 1%-settling times (t_{IE}, t_{NIE}) are considered, computed as $t_i = \tau_i + 5T_i, i \in \{IE, NIE\}$; this last parameter is useful in evaluating the overall pupil reactivity, since it takes into account both the delay time and the time constant. All the described features are time-related and express dynamic characteristic of the pupillary response, except for the gains μ_{IE} and μ_{NIE} which are the only static features.

V. Experimental Results

This Section presents the results of experimental tests performed on three different subjects. First, the time profiles of the pupillary responses are shown for both the IE and NIE; then, the considered features are computed for each subject and compared to each other, in order to draw conlusions on their values and on their intra- and inter-subject variability.

A. Time-domain analysis

Figg. 4 and 5 show the time profiles of the pupillary responses (IE and NIE respectively) of three subjects immediately after the light stimulus application.

From Fig. 4, we notice the IE's pupil to range from 40% to 60% of the iris size in dark condition, reducing to $[25,40]$% after the light stimulus application. While Subjects 1 and 2 have similar pupil sizes, Subject 3 presents significantly smaller pupil, which highlights a consistent inter-subject pupil diameter variability. Similarly, in terms of

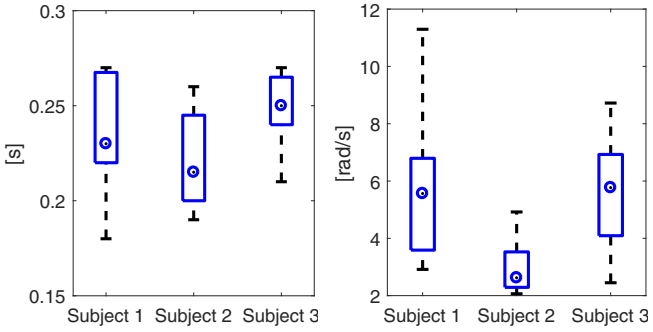

(a) Delay - τ_{IE}

(b) Pole Frequency - ω_{IE}

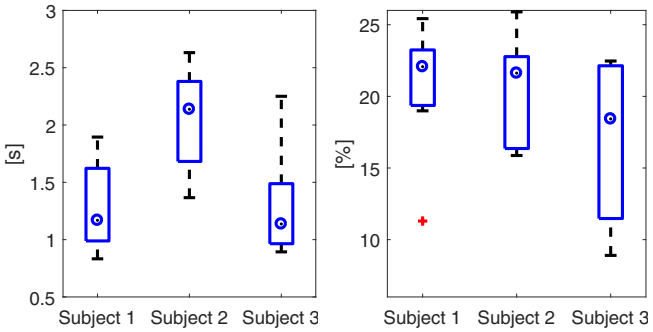

(c) Settling Time - t_{IE}

(d) Gain - μ_{IE}

Fig. 6: Features - Illuminated Eye

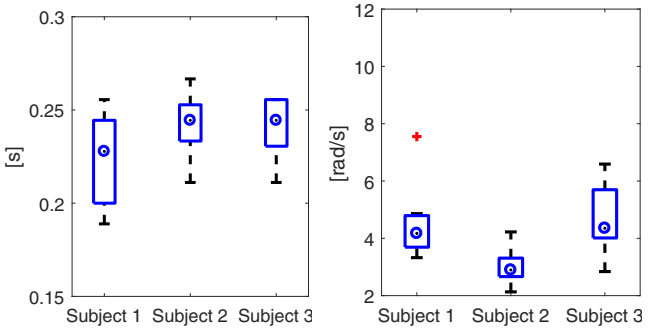

(a) Delay - τ_{NIE}

(b) Pole Frequency - ω_{NIE}

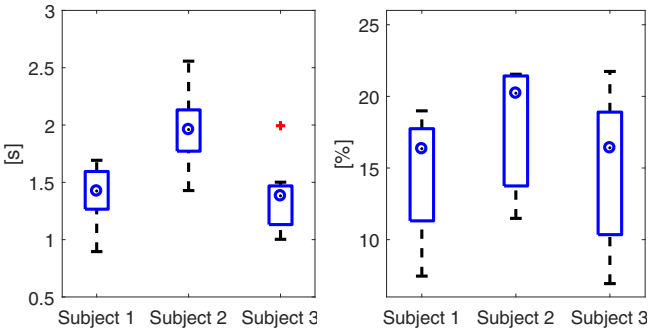

(c) Settling Time - t_{NIE}

(d) Gain - μ_{NIE}

Fig. 7: Features - Not Illuminated Eye

intra-subject variability, the three persons exhibit different behavior; Subject 2 presents very high repeatability, with the three profiles being almost perfectly superimposed. On the other hand, for Subject 1 the three profiles are slightly different, while Subject 3 presents great variability (more than 10% difference in dark condition). Finally, the dynamics can considered to be expired for the three subjects after around 1.5%.

Fig. 5 shows the behavior of the NIEs: as expected, the not illuminated pupils constrict due to the Consensual Light Reflex, following the same dynamics as the respective IEs. The same considerations about inter- and intra-subject variability can be made, with respect to the IE, except for Subject 2 being slightly more variable.

In conclusion, the time profiles of the considered PLRs can be fairly well approximated by responses of 1^{st}-order system with time delay. Poor repeatability has been found in general for different tests made by the same subject, both for the IE and NIE; moreover, different subjects generally present significantly different behavior, hence a statistical analysis of the extracted features is performed in the following.

B. Features Analysis

The entire population of the acquired step responses is subdivided by subject, and for each subject the eight features of the vector φ are computed. Fig. 6 contains the features relative to the illuminated eye, while Fig. 7 refers to the not illuminated eye, each box representing a 9-elements population of step responses. For each box, the interval delimited by the dashed lines contains all elements of the population not considered as outliers; the rectangles encase all elements within 25^{th} and 75^{th} quantile (which is a measure of the intra-subject variability) and the small circles within the boxes indicate the median of the population. The comparison of the median values of different subjects quantifies the inter-subject variability.

The delay feature is represented in Figg. 6a and 7a for the IE and NIE respectively. From both plots, the median values appear to be fairly close to each other, ranging in $[0.22, 0.25]\,s$; the highest intra-subject variability is found in the IE of Subject 1, whose delay varies in the $[0.18, 0.27]\,s$ interval.

The pole frequencies (Figg. 6b and 7b) are found to be less variable in the NIE; in general, the median values of this feature are strongly variable, ranging within the $[2.5, 5.8]\,rad/s$ interval and again the highest intra-subject variability appears in Subject 1's IE, whose pole frequency vary within the $[3, 11.5]\,rad/s$ interval.

Figg. 6c and 7c regard the settling time, whose median ranges in $[1.2, 2.2]\,s$; this feature globally present a huge intra-subject variability as, for example, in Subject 2's IE ($[1.4, 2.7]\,s$).

Finally, the gain feature (Figg. 6d and 7d) is expressed in terms of percentage of iris diameter and presents a high intra-subject variability for each subject: the greatest is Subject 3's IE, with variations within $[8, 22]\,\%$. For the considered subjects, the median values range within $[17, 22]\,\%$.

To conclude, eight features have been extracted from a small, not statistically relevant set of subjects (which is

out of scope for this study); however, the results reveal a consistent variability depending on the person, where also single subjects exhibit significantly different behavior in different measurements. These results are easily expected to hold also for bigger sets of persons and are representative of the intra- and inter-subject variability of the evaluated properties.

The above considerations lead to the following conclusions:

- due to the inter-subject variability, the design of a robust DDDS requires a specific tuning for each particular subject.
- due to the intra-subject variability, the design of a simple threshold-based DDDS that compares one of the features extracted from a single PLR acquisition to a baseline value results not to be robust enough.

The abovementioned conclusions lead to the proposal of two DDDS strategies, which are tuned *ad-hoc* on the particular driver:

1) a statistics-based DDDS is designed, which acquires a set of PLRs from the driver and computes the median value of one feature (the response delay results to be the less varying parameter); the drowsiness condition is detected by comparing this value with the medians of two populations previously acquired in normal and drowsy conditions.
2) a neural network-based DDDS is designed, trained on a set of PLRs acquired in normal and drowsy condition, which classifies a single PLR acquired from the driver into one of the two conditions exploiting pattern-recognition methods.

VI. Conclusions

This study presents a low-cost methodology for extracting dynamic and static characteristics of subject's PLRs from video sequences. The required hardware consists in a couple of cameras recording at $100\,fps$, a standard one and a full-spectrum one equipped with IR filter to enhance infrared-content. A light stimulus is applied to one eye, whose pupil constriction dynamics is recorded with the standard camera, while for the not illuminated eye the IR camera is used. A simple CHT-based methodology is proposed for extracting pupil diameter profiles from the video sequences, which are used to fit a 1^{st}-order model and extract some static and dynamic features.

The time-domain analysis showed that the observed dynamics can be fairly well approximated as responses of a 1^{st}-order system; however, both the time-domain and feature analysis of the obtained PLRs performed on three subjects revealed consistent intra- and inter-subject variability of the PLRs both in static and dynamic terms. For this reason, two DDDS solutions have been proposed, a statistics-based and a neural network-based one, that will be implemented and presented as a future work.

References

[1] "The top 10 causes of death," http://www.who.int/mediacentre/factsheets/fs310/en/.

[2] J. A. Horne and L. A. Reyner, "Sleep related vehicle accidents," *Bmj*, vol. 310, no. 6979, pp. 565–567, 1995.

[3] P. Philip, F. Vervialle, P. Le Breton, J. Taillard, and J. A. Horne, "Fatigue, alcohol, and serious road crashes in france: factorial study of national data," *Bmj*, vol. 322, no. 7290, pp. 829–830, 2001.

[4] A. Ziebinski, R. Cupek, H. Erdogan, and S. Waechter, "A survey of adas technologies for the future perspective of sensor fusion," in *International Conference on Computational Collective Intelligence*. Springer, 2016, pp. 135–146.

[5] P. Gáspár, Z. Szabó, J. Bokor, and B. Németh, "Adaptive cruise control in longitudinal dynamics," in *Robust Control Design for Active Driver Assistance Systems*. Springer, 2017, pp. 135–158.

[6] M. Alirezaei, M. Corno, D. Katzourakis, A. Ghaffari, and R. Kazemi, "A robust steering assistance system for road departure avoidance," *IEEE Transactions on Vehicular Technology*, vol. 61, no. 5, pp. 1953–1960, 2012.

[7] A. Amodio, G. Panzani, and S. M. Savaresi, "Design of a lane change driver assistance system, with implementation and testing on motorbike," in *2017 IEEE Intelligent Vehicles Symposium June 11-14*, 2017.

[8] "The COMPASS Handbook of ICT Solutions," http://81.47.175.201/compass/.

[9] F. Rohit, V. Kulathumani, R. Kavi, I. Elwarfalli, V. Kecojevic, and A. Nimbarte, "Real-time drowsiness detection using wearable, lightweight brain sensing headbands," *IET Intelligent Transport Systems*, vol. 11, no. 5, pp. 255–263, 2017.

[10] S. M. R. Noori and M. Mikaeili, "Driving drowsiness detection using fusion of electroencephalography, electrooculography, and driving quality signals," *Journal of medical signals and sensors*, vol. 6, no. 1, p. 39, 2016.

[11] Y.-P. Huang, N. N. Sari, and T.-T. Lee, "Early detection of driver drowsiness by wpt and flfnn models," in *Systems, Man, and Cybernetics (SMC), 2016 IEEE International Conference on*. IEEE, 2016, pp. 000 463–000 468.

[12] T. Hwang, M. Kim, S. Hong, and K. S. Park, "Driver drowsiness detection using the in-ear eeg," in *Engineering in Medicine and Biology Society (EMBC), 2016 IEEE 38th Annual International Conference of the*. IEEE, 2016, pp. 4646–4649.

[13] G. Zhenhai, L. DinhDat, H. Hongyu, Y. Ziwen, and W. Xinyu, "Driver drowsiness detection based on time series analysis of steering wheel angular velocity," in *Measuring Technology and Mechatronics Automation (ICMTMA), 2017 9th International Conference on*. IEEE, 2017, pp. 99–101.

[14] J.-J. Yan, H.-H. Kuo, Y.-F. Lin, and T.-L. Liao, "Real-time driver drowsiness detection system based on perclos and grayscale image processing," in *Computer, Consumer and Control (IS3C), 2016 International Symposium on*. IEEE, 2016, pp. 243–246.

[15] A. Mittal, K. Kumar, S. Dhamija, and M. Kaur, "Head movement-based driver drowsiness detection: A review of state-of-art techniques," in *Engineering and Technology (ICETECH), 2016 IEEE International Conference on*. IEEE, 2016, pp. 903–908.

[16] F. Onorati, R. Barbieri, M. Mauri, V. Russo, and L. Mainardi, "Characterization of affective states by pupillary dynamics and autonomic correlates," *Frontiers in neuroengineering*, vol. 6, 2013.

[17] L. E. Baker, "The pupillary response conditioned to subliminal auditory stimuli." *Psychological Monographs*, vol. 50, no. 3, p. i, 1938.

[18] V. F. Pamplona, M. M. Oliveira, and G. V. Baranoski, "Photorealistic models for pupil light reflex and iridal pattern deformation," *ACM Transactions on Graphics (TOG)*, vol. 28, no. 4, p. 106, 2009.

[19] A. Czajka, "Pupil dynamics for iris liveness detection," *IEEE Transactions on Information Forensics and Security*, vol. 10, no. 4, pp. 726–735, 2015.

[20] H. T. Ngo, R. N. Rakvic, R. P. Broussard, and R. W. Ives, "Resource-aware architecture design and implementation of hough transform for a real-time iris boundary detection system," *IEEE Transactions on Consumer Electronics*, vol. 60, no. 3, pp. 485–492, 2014.

[21] R. G. Bozomitu, A. Păsărică, V. Cehan, C. Rotariu, and C. Barabaşa, "Pupil centre coordinates detection using the circular hough transform technique," in *Electronics Technology (ISSE), 2015 38th International Spring Seminar on*. IEEE, 2015, pp. 462–465.